Electromagnetic Coupling in a dc Motor and Tachometer Assembly

Shorya Awtar[1]

Doctoral Candidate, Department of Mechanical Engineering, Massachusetts Institute of Technology, 77 Massachusetts Avenue, No. 3-470, Cambridge, MA 02139
e-mail: shorya@mit.edu

Kevin C. Craig

Associate Chair for Graduate Studies and Associate Professor, Department of Mechanical, Aerospace and Nuclear Engineering, Rensselaer Polytechnic Institute, 110 8th Street, Troy, NY 12180
e-mail: craigk@rpi.edu

This paper presents an enhanced tachometer model that takes into account the effect of electromagnetic coupling that can exist between the actuator and sensor in an integrated dc motor-tachometer assembly, where the conventional model is found to be inadequate. The tachometer dynamics identified in this paper is experimentally verified, and incorporated in the modeling and parameter identification of a motion system that has multiple flexible elements. It is shown that the tachometer dynamics contributes additional nonminimum phase zeros that degrade the servo system performance in terms of closed-loop bandwidth, disturbance rejection and sensitivity to modeling uncertainty. The zeros of the open loop system are found to vary with the geometric parameters of the motor-tachometer assembly. Based on the insight gained by modeling the electromagnetic coupling, methods for eliminating it and its resulting detrimental effects are also suggested.
[DOI: 10.1115/1.1789543]

Keywords: Servomotor Control, Tachometer Model, Sensor Actuator Crosstalk, Electromagnetic Coupling, Zero-Locus

1 Introduction and Background

Closed-loop control of a dc motor to drive load inertia is a common industrial and research application. Very often, dc tachometers are used to provide velocity feedback for motion control [1–3]. In the presence of flexible components in the drive system, for example, a compliant motor-tachometer shaft or a flexible mechanical coupling, this exercise in servo-control design becomes quite challenging [4–8]. Furthermore, a perfect feedback of relevant states may not be available, and the sensors may pick up erroneous signals from other components in the servosystem, resulting in additional dynamics. By means of an illustrative example, it is shown in this paper that an accurate model of the sensor dynamics is critical in determining the limits of closed-loop bandwidth and system performance, and therefore should be incorporated in the overall system model before a compensator is designed.

The motivation for this work comes from an experimental frequency response measurement of a motor-tachometer system, that did not match initial analytical predictions based on the conventional models of dc machines. The experimental test setup consists of an integrated permanent magnet dc motor-tachometer unit from Electro-Craft (Part No. 0288-32-003). Both the motor and tachometer in this assembly are two-pole permanent magnet stator devices. A shaft of finite stiffness connects the tachometer and motor armatures. A voltage-to-current PWM servo-amplifier is employed to operate the motor in current mode. The amplifier transfer function, between command voltage and motor current, is experimentally obtained to be,

$$\frac{I_1}{V_{in}} = \frac{K_{amp}}{(\tau_{amp}s+1)}. \tag{1}$$

The open-loop system output, tachometer voltage signal V_{tach}, can be used for system identification or for feedback in motion control. Experimental open-loop frequency response between V_{in} and V_{tach} is obtained using a dynamic signal analyzer, SigLab, from DSP Technology Inc. To characterize the dc motor-tachometer unit by itself, no external load inertia was attached to the output shaft in the initial experiments. A lumped parameter model of this mechanical assembly was used to obtain the transfer function between the motor torque input and the tachometer rotor angular position:

$$\frac{\theta_t}{T_{motor}} = \frac{K}{s^2[J_t J_m s^2 + K(J_t + J_m)]}. \tag{2}$$

The following conventional models for dc motor and tachometer, commonly found in the literature [9,10], were used at this stage:

$$T_{motor} = K_{t\_motor} I_1 \qquad V_{tach} = K_{b\_tach} \dot{\theta}_t. \tag{3}$$

Using Eqs. (1)–(3), the overall system transfer function was derived to be

$$\frac{V_{tach}}{V_{in}} = \frac{K_{amp} K_{b\_tach} K_{t\_motor} K}{s[J_t J_m s^2 + K(J_t + J_m)](\tau_{amp}s+1)}. \tag{4}$$

The open-loop system frequency response predicted by this transfer function was then compared to the experimentally obtained frequency response, both of which are plotted in Fig. 1. While the experimental results agree with the analytical predictions in the low frequency range, there is a significant deviation at frequencies above 100 Hz. The model derived above clearly fails to predict the experimentally observed system zeros. Furthermore, an unexplained phase drop of 180° can be seen at the first zero frequency in the experimental frequency response plot. This indicates that the corresponding complex conjugate zero pair lies in the right half plane (RHP), thereby making the system nonminimum phase.

The above discrepancies called for a closer inspection of the system modeling. Neglecting dissipative effects and assuming lumped parameters would not normally cause additional dynamics in the system response. Any possible amplifier dynamics, in the frequency range of interest, is already captured in Eq. (1). The extra zeros and their nonminimum phase nature revealed in the experimental frequency response measurement indicated that there was some physical phenomenon in the system that had not been adequately modeled. Since, the motor and tachometer expressions (3) represent textbook models of idealized electromagnetically isolated dc machines, it was suspected that these might be oversimplifications for the pertinent analysis, and therefore demanded a careful reconsideration. The ensuing investigation, its findings and the consequences of these findings are presented in the this paper. Section 2 covers the basic background on modeling dc machines and extends this to an integrated motor-tachometer assembly. The analytical findings of Sec. 2 are experimentally verified and qualitatively discussed in Sec. 3. Section 4 addresses the motion control problem in the presence of drive system compliance and sensor dynamics, the paper concludes with Sec. 5.
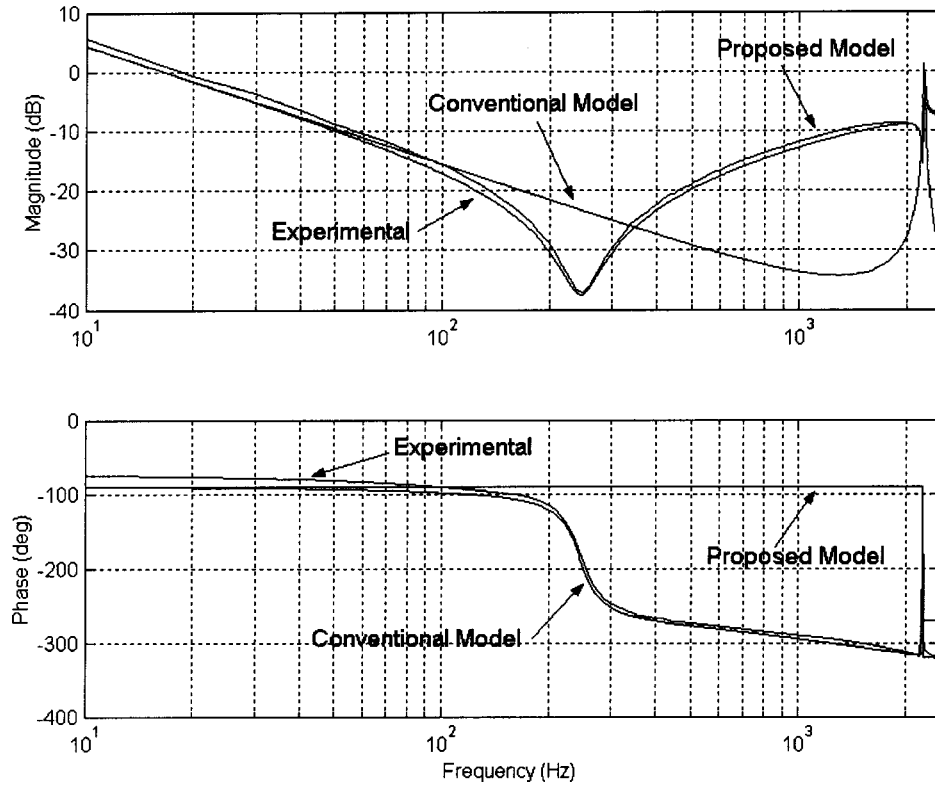
Fig. 1 V_{tach}/V_{in} **Bode plot for the motor-tachometer system: Experimental measurement, conventional model, and proposed model**

2 Modeling an Integrated dc Motor-Tachometer Assembly

In the case of a dc motor, commutation ensures that the armature current produces an armature field that retains its orientation in space and is always perpendicular to the stator field. The motor armature then behaves like a magnetic dipole, and therefore experiences a counter clockwise torque in the presence of the stator field, which can be shown to be

$$T_{\text{motor}} = (N_1 A_1 B_{m1}) I_1 \triangleq K_{t\_\text{motor}} I_1. \tag{5}$$

The *backemf* generated in the motor coil rotating in a radially uniform stator field is given by

$$V_{b\_\text{motor}} = (N_1 A_1 B_{m1}) \omega_m \triangleq K_{b\_\text{motor}} \omega_m. \tag{6}$$

Application of the laws of electromagnetism yields the following motor circuit relationship;

$$V_1 - V_{b\_\text{motor}} - N_1 \frac{d\Phi_{11}}{dt} = R_1 I_1 \Rightarrow V_1 - K_{b\_\text{motor}} \omega_m - M_{11} \frac{dI_1}{dt}$$

$$= R_1 I_1. \tag{7}$$

Similar relationships hold for a dc tachometer:

$$V_{b\_\text{tach}} = (N_2 A_2 B_{m2}) \omega_t \triangleq K_{b\_\text{tach}} \omega_t,$$

$$T_{\text{tach}} = (N_2 A_2 B_{m2}) I_2 \triangleq K_{t\_\text{tach}} I_2. \tag{8}$$

In this case, T_{tach} is a retarding torque resulting from the armature current, and opposes the rotation of the tachometer rotor. Laws of electromagnetism applied to the tachometer electrical circuit result in

$$V_{b\_\text{tach}} - N_2 \frac{d\Phi_{22}}{dt} = (R_2 + R_L) I_2 \Rightarrow K_{b\_\text{tach}} \omega_t - M_{22} \frac{dI_2}{dt}$$

$$= (R_2 + R_L) I_2. \tag{9}$$

The terminal voltage as seen by a load resistor R_L is given by

$$V_{\text{tach}} = R_L I_2 = K_{b\_\text{tach}} \omega_t - M_{22} \frac{dI_2}{dt} - R_2 I_2. \tag{10}$$

When R_L is very large, the current, I_2, drawn from the tachometer terminals is negligible and the above expression simply reduces to $V_{\text{tach}} = K_{b\_\text{tach}} \omega_t$. Expressions (5)–(7) and (8)–(10) represent the conventional models for an "electromagnetically isolated" dc motor and tachometer, respectively [9,10].

We now consider a mechanically coupled motor and tachometer placed in close proximity, like the system shown in Fig. 2. In general, there can be an angular offset, say α, between the motor stator poles and the tachometer stator poles. $\boldsymbol{B_{m1}}$ and $\boldsymbol{B_{m2}}$ are the motor and tachometer stator fields, and $\boldsymbol{B_{a11}}$ and $\boldsymbol{B_{a22}}$ are the motor and tachometer armature fields, respectively. The directions of $\boldsymbol{B_{m1}}$ and $\boldsymbol{B_{m2}}$ are defined by the orientation of the permanent magnet stators, and the directions of $\boldsymbol{B_{a11}}$ and $\boldsymbol{B_{a22}}$ can be determined to be perpendicular to the respective stator fields. Since the two devices are not magnetically insulated, the tachometer armature sees a weak field $\boldsymbol{B_{a12}}$, due to the motor armature current I_1. $\boldsymbol{B_{a12}}$ acts along the same line as $\boldsymbol{B_{a11}}$, but is opposite in direction since magnetic flux exists in closed paths. The tachometer also experiences a weak field $\boldsymbol{B_{m12}}$, resulting from the leakage flux of the permanent magnets of the motor and hence is in the same direction as $\boldsymbol{B_{m1}}$. In a similar fashion, the motor armature experiences a magnetic field $\boldsymbol{B_{a21}}$, due to the current I_2 in the tachometer armature. Once again, the direction of $\boldsymbol{B_{a21}}$ is opposite to the direction of $\boldsymbol{B_{a22}}$. The effect of the tachometer permanent magnets as seen by the motor is a weak field, $\boldsymbol{B_{m21}}$, acting in the direction of $\boldsymbol{B_{m1}}$.

The effect of $\boldsymbol{B_{m12}}$ on the tachometer equations and $\boldsymbol{B_{m21}}$ on the motor equations, is negligible since these fields do not lead to any additional dynamic effects. They simply result in a small static variation in the torque and *backemf* constants of the two devices.
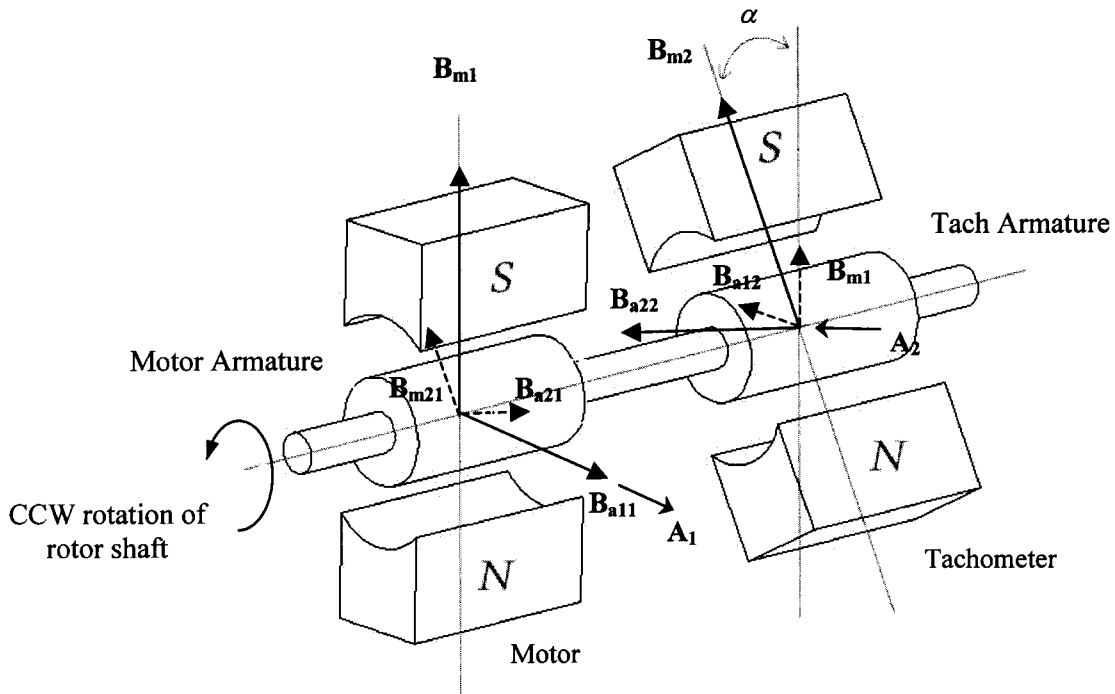
Fig. 2   Angular orientations of the motor and tachometer permanent magnets

Nevertheless, the relationships given by Eqs. (5), (6), and (8) remain unaltered. The presence of the auxiliary armature fields, B_{a12} and B_{a21}, leads to mutual inductance between the two armature coils. It is important to visualize that although the armatures are rotating physically, commutation in the two devices ensures that the respective directions of all the fields remain fixed in space. Therefore, the mutual inductance phenomenon between the rotating motor and tachometer armatures can be analyzed while treating the two armatures as static in an electromagnetic sense, with area vectors pointing in the direction of the respective armature fields.

In this case, there is a very weak transformer effect quite unlike an *ideal* transformer. In an *ideal* transformer, winding resistance and core hysteresis losses are negligible, permeability of the core is infinitely high, and all the flux is confined to the core thus linking both the coils. The following input-output relations hold for such an *ideal* transformer when the excitation is sinusoidal [11]:

$$\frac{V_2}{V_1}=\frac{N_2}{N_1} \quad \text{and} \quad \frac{I_2}{I_1}=\frac{N_1}{N_2} \tag{11}$$

Clearly, the present case, as illustrated in Fig. 3, is very different from an *ideal* transformer. There is no core between the two coils and the permeability of air is very low. Most part of the flux linked with each coil is 'leakage' flux, and the mutual flux is small. Moreover, there is a mechanical power outlet on the primary side as a consequence of motor action, and an additional voltage source on the secondary side resulting from generator action. Since these issues are not accounted for in the standard transformer analysis, the relationships (11) are obviously not valid for the motor-tachometer case. To analyze the present problem, it therefore becomes necessary to start from the fundamentals, and make simplifying assumptions where appropriate.

Ampere's Law requires the magnitudes of the armature fields to be linearly dependent on the respective armature currents as long as magnetic saturation is not reached:

$$B_{aij}=k_{ij}I_i, \tag{12}$$

where k_{ij} are constants that depend on material magnetic properties and geometry of the arrangement. In Fig. 3, Φ_{ij} is the flux linkage in coil j due to current in coil i, and is given by

$$\Phi_{ij}=B_{aij}\cdot A_j. \tag{13}$$

The resultant flux linkage in motor armature $(\text{coil1})=\Phi_{11}+\Phi_{21}$ and, the resultant flux linkage in tachometer armature (coil2) $=\Phi_{22}+\Phi_{12}$. Applying laws of electromagnetism to the electrical circuit comprising the motor armature, and the electrical circuit comprising the tachometer armature, results in

$$V_1-V_{b\_motor}-N_1\frac{d(\Phi_{11}+\Phi_{21})}{dt}=R_1l_1, \tag{14}$$

$$V_{b\_tach}-N_2\frac{d(\Phi_{22}+\Phi_{12})}{dt}=(R_2+R_L)I_2. \tag{15}$$

Both equations now have an additional mutual flux term. The physical significance and sign of each term that appears in the above equations can be explained by Faraday's and Lenz's Laws. Employing Eqs. (12) and (13), one can next define inductances:

$$N_j\Phi_{ij}=N_j(B_{aij}\cdot A_j)\triangleq M_{ij}I_i. \tag{16}$$

It can be shown that, $M_{11}=N_1A_1k_{11}$, $M_{22}=N_2A_2k_{22}$, $M_{21}=N_1A_1k_{21}\cos(\alpha)$, and $M_{12}=N_2A_2k_{12}\cos(\alpha)$. Based on the requirements imposed by Maxwell's Reciprocity, we can further express the mutual inductance as,

$$M_{12}=M_{21}\triangleq M\cos(\alpha).$$

Using the previously stated relations, $V_{b\_motor}=K_{b\_motor}\omega_m$ and $V_{b\_tach}=K_{b\_tach}\omega_t$, which are still valid, and expressions (16), the motor Eq. (14) reduces to

$$V_1-K_{b\_motor}\omega_m-L_1\frac{dI_1}{dt}-M\cos(\alpha)\frac{dI_2}{dt}=R_1I_1, \tag{17}$$

and the tachometer Eq. (15) reduces to
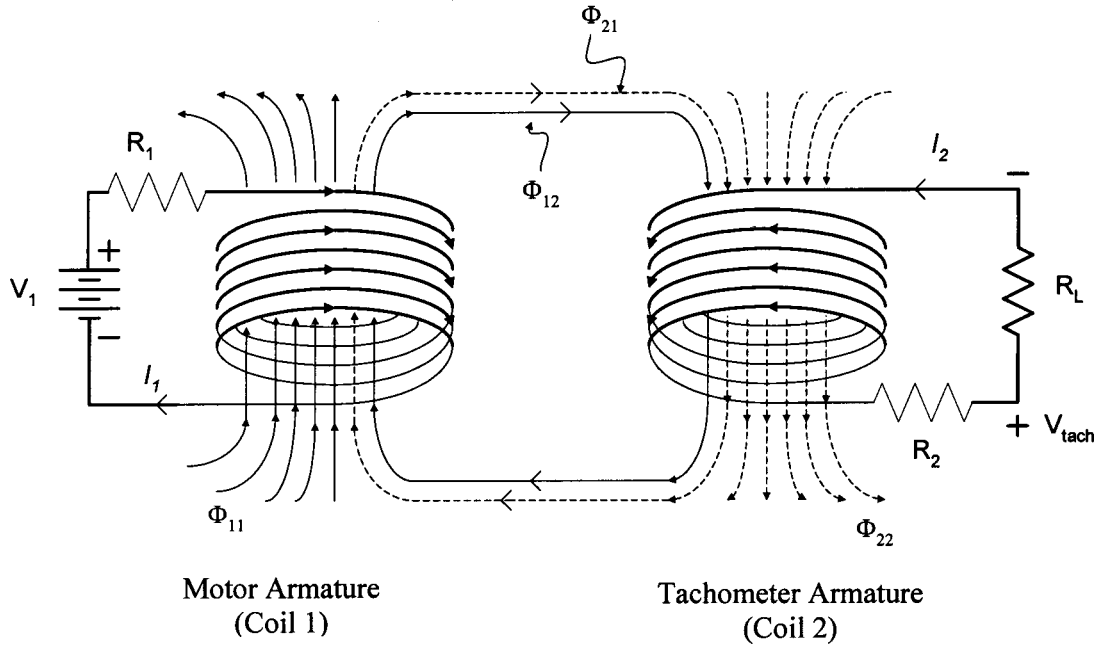
Fig. 3 Transformer effect between the motor armature coil and tachometer armature coil

$$K_{b\_\text{tach}}\omega_t - L_2\frac{dI_2}{dt} - M\cos(\alpha)\frac{dI_1}{dt} = (R_2 + R_L)I_2,$$
(18)

$$\Rightarrow V_\text{tach} = R_L I_2 = K_{b\_\text{tach}}\omega_t - L_2\frac{dI_2}{dt} - M\cos(\alpha)\frac{dI_1}{dt} - R_2 I_2.$$

Torque models for the motor and tachometer are the same as presented earlier in this section, and are not affected by the proximity of the motor and tachometer. Thus, the net torque output by the motor-tachometer assembly is

$$T_\text{out} = K_{t\_\text{motor}}I_1 - K_{t\_\text{tach}}I_2.$$
(19)

At this stage in the derivation, some simplifications may be considered. A practical observation is that the load current I_2 is much smaller than the motor current I_1 since the input impedance, R_L, of voltage measuring devices is typically very high ($\sim$1 MΩ). We can therefore consider dropping the terms containing I_2, wherever they occur in Eqs. (17)–(19). However, we propose to retain the term "$-R_2 I_2$" in the V_tach expression (18). As shall be seen in later derivations, although this term is insignificant for the low frequency response, it contributes to the damping of the system zeros that occur at higher frequencies. For some cases, the sign associated with this damping term can become crucial in determining whether the system is nonminimum phase or not. It may be recalled that the initial experimental measurements indicated negative damping being associated with some of the system zeros, an observation that can possibly be explained by retaining the $-R_2 I_2$ term, however small, because of its negative sign.

We now make a final observation regarding the weak transformer effect that was mentioned earlier. Clearly, the motor tachometer interaction is far from an *ideal* transformer in general, but in the high frequency region it may be fairly approximated by a *nonideal transformer* [11]. Since the motor and tachometer rotor velocities are significantly attenuated for high frequency motor current excitation, it can be safely assumed that the motor and generator effects are negligible at these frequencies. Furthermore, the excitation input is obviously sinusoidal at high frequencies. Given these conditions, the motor tachometer can be treated as a *nonideal transformer* with finite core reluctance and leakage flux. For this nonideal case, it can be shown that

$$\frac{I_2}{I_1} \simeq \eta\frac{N_1}{N_2},$$
(20)

where η represents the strength of the transformer effect and is defined as the portion of flux generated by one coil reaching the other coil [12]. Therefore, in the present case

$$\eta = \frac{\Phi_{12}}{\Phi_{11}} = \frac{\Phi_{21}}{\Phi_{22}} = \left[\frac{M^2\cos^2(\alpha)}{M_{11}M_{22}}\right]^{1/2}.$$
(21)

Further algebraic manipulation leads to

$$I_2 = \frac{N_1}{N_2}\frac{M}{\sqrt{M_{11}M_{22}}}|\cos(\alpha)|I_1 \Rightarrow R_2 I_2 = R|\cos(\alpha)|I_1,$$
(22)

where

$$R \triangleq R_2\frac{N_1}{N_2}\frac{M}{\sqrt{M_{11}M_{22}}}.$$

Incorporating these approximations, the motor-tachometer equations resolve to,

Motor equation: $$V_1 - K_{b\_\text{motor}}\omega_\text{m} - M_{11}\frac{dI_1}{dt} = R_1 I_1$$

Tachometer equation: $$V_\text{tach} = K_{b\_\text{tach}}\omega_t - M\cos(\alpha)\frac{dI_1}{dt}$$
$$- R|\cos(\alpha)|I_1.$$
(23)

Torque equation: $$T_\text{out} = K_{t\_\text{motor}}I_1$$

Comparing these with the previously presented conventional models, it is seen that the motor model and the torque expression remain the same. Noticeably, the new tachometer model has additional terms that are not present in the conventional model. Rewriting the tachometer equation with $-M\cos(\alpha) \triangleq K_m$, and $R|\cos(\alpha)| \triangleq K_r$,

$$V_\text{tach} = K_{b\_\text{tach}}\omega_t + K_m\frac{dI_1}{dt} - K_r I_1.$$
(24)

This is the final form of the enhanced tachometer model presented in this paper. K_m and K_r are defined as the *electromagnetic coupling constant* and *loading effect constant*, respectively.

3 Experimental Verification and Key Attributes of the Proposed Model

The tachometer model derived in Sec. 2 can now be incorporated in the analysis of the motor-tachometer electromechanical system described in Sec. 1. As earlier, there is no load inertia connected to the system. Using Eqs. (1), (2), and (23), the overall open-loop transfer function for the motor-tachometer electromechanical system is,

$$\frac{V_{\text{tach}}}{V_{in}} = \frac{K_{\text{amp}}[K_m(\text{den})s^2 - K_r(\text{den})s + K_{t\_\text{motor}}K_{b\_\text{tach}}K]}{(\text{den})s}.$$
(25)

where,

$$(\text{den}) \triangleq [J_t J_m s^2 + K(J_t + J_m)]$$

It is immediately clear that this transfer function is different from the previously obtained transfer function (4), which was based on the conventional tachometer model. If K_m and K_r were to be zero, the two transfer functions become identical. A comparison between analytical predictions based on Eq. (25) and experimental measurements is presented in Fig. 1, which shows that all the discrepancies that exist between the conventional model and experimental measurements are resolved by the proposed motor-tachometer model.

The most important feature of the new tachometer model is the presence of an electromagnetic coupling constant, $K_m \triangleq -M\cos\alpha$, which is simply the mutual inductance between the two armature coils. It directly links the tachometer voltage to the motor current. Because of the electromagnetic coupling term, the denominator of the mechanical system transfer function finds a place in the numerator of the overall system transfer function, as is evident in expression (25), thus resulting in additional system zeros. Furthermore, these additional zeros are strongly dependent on the system poles, thereby making the effect of the tachometer dynamics system dependent.

The other important parameter that appears in the proposed tachometer expression is the loading effect constant, $K_r \triangleq R|\cos\alpha|$, which is always positive. Being very small, K_r has an insignificant effect on the magnitude of the frequency response. Importantly though, when the additional zeros are complex conjugate, the negative sign associated with K_r pushes some of these zeros into the right half of s plane. This phenomenon helps in explaining the 180° phase drop at some of the zero frequencies in the phase plot. Thus, the presence of K_r makes the system nonminimum phase, which significantly affects the closed-loop performance. This is an interesting find because complex zeros in the RHP are uncommon in purely mechanical systems.

As the preceding analysis indicates, it is difficult to calculate the constants K_m and K_r because of their dependence on the material magnetic properties and the geometry of the motor-tachometer arrangement. Experimental estimates of K_m and K_r are obtained by locking the motor and tachometer rotors in place, and supplying a regulated sinusoidal current of a known high frequency to the motor armature. Because of the coupling effects described above, a voltage is generated across the tachometer terminals. The component of the generated voltage that is in phase with the excitation current provides an estimate of K_r, and the component that is 90° out of phase with the excitation provides an estimate of K_m. For the given motor-tachometer, in its factory assembled state, K_m is determined to be 8.62565×10^{-5} Henry and K_r is determined to be 2.6656×10^{-2} Ω. It is noteworthy that although K_m and K_r are very small numbers, they significantly affect the high frequency system dynamics.

Since the angle α has a significant influence on the resulting system zeros, and therefore the closed-loop system performance, a locus of system zeros obtained by varying the angle α proves to be very insightful. Such a zero-locus for the motor-tachometer system is presented in Fig. 4. It should be recognized that the zeros of the closed-loop system are the same as the zeros of the open-loop system. If $\alpha = 0°$, then K_m is maximum negative and K_r is maximum positive, which leads to additional zeros—a complex conjugate pair close to the system poles, and a real pair placed symmetrically about the imaginary axis, resulting in a nonminimum phase system. As the angle is increased to 90°, all these zeros move out to infinity since the effect of the tachometer dynamics gradually vanishes. As the angle is further varied from 90° to 180° the mutual inductance increases, and new system zeros reappear approaching from infinity. For $\alpha = 180°$, both K_m and K_r are maximum positive, which leads to two additional pairs of complex-conjugate zeros—one pair that lies close to the system poles, and another that is at a much lower frequency. This latter pair falls on the right side of the imaginary axis, and once again the system is nonminimum phase. The significance of the signs associated with K_r and K_m is evident since these signs dictate the nature and location of the added zeros.

4 Implications on Motion Control Design

We next proceed to consider a servo system design using the dc motor-tachometer assembly described in Sec. 1, so as to determine the extent by which the above identified sensor–actuator interaction changes the system dynamics and affects closed-loop performance. As illustrated in Fig. 5, a flexible coupling now connects the motor shaft to a load inertia, which is in the form of two inertia elements mounted on a compliant shaft. A lumped parameter model is used to describe the mechanical system, and results in the following transfer function between the tachometer angle and motor torque:

$$\frac{\theta_t}{T_m} = \frac{(\text{num})}{s^2 \cdot (\text{den})}$$
(26)

where,

$$(\text{num}) = K[J_1 J_2 s^4 + (J_1 K_2 + J_2 K_1 + J_2 K_2)s^2 + K_1 K_2],$$

and

$$(\text{den}) = s^6[J_t J_m J_1 J_2] + s^4[K_2 J_t J_m J_1 + K_1 J_t J_m J_2 + K_2 J_t J_m J_2 \\ + K J_m J_1 J_2 + K J_t J_1 J_2 + K_1 K_t J_1 J_2] + s^2[K_1 K_2 J_t J_m \\ + K K_2 J_1 J_m + K K_1 J_2 J_m K K_2 J_2 J_m + K K_2 J_t J_1 \\ + K K_1 J_t J_2 K K_2 J_t J_2 + K_1 K_2 J_t J_1 + K K_1 J_1 J_2 + K_1 K_2 J_1 J_2] \\ + [K K_1 K_2 (J_t + J_m + J_1 + J_2)].$$

Although not shown in the above model, mechanical damping in the system is assumed to be viscous in nature. Using the enhanced motor-tachometer model (23) the following overall system transfer function can be obtained:

$$\frac{V_{\text{tach}}}{V_{in}} = \frac{K_{\text{amp}}[K_m s^2(\text{den}) - K_r s(\text{den}) + K_{t\_\text{motor}}K_{b\_\text{tach}}(\text{num})]}{s(\text{den})(\tau_{\text{amp}}s + 1)}.$$
(27)

Once again, a sine-sweep experiment is performed on the actual system to obtain its frequency response. The experimentally obtained frequency response is compared with that predicted by the conventional model and the proposed model in Fig. 6. The open-loop system response based on the proposed tachometer model matches the experimental measurement almost exactly in terms of the magnitude and phase variations over the entire frequency range. On the other hand, as was expected, the conventional modeling fails in predicting the system zeros and their nonminimum phase nature. Open-loop complex conjugate poles and zeros of the
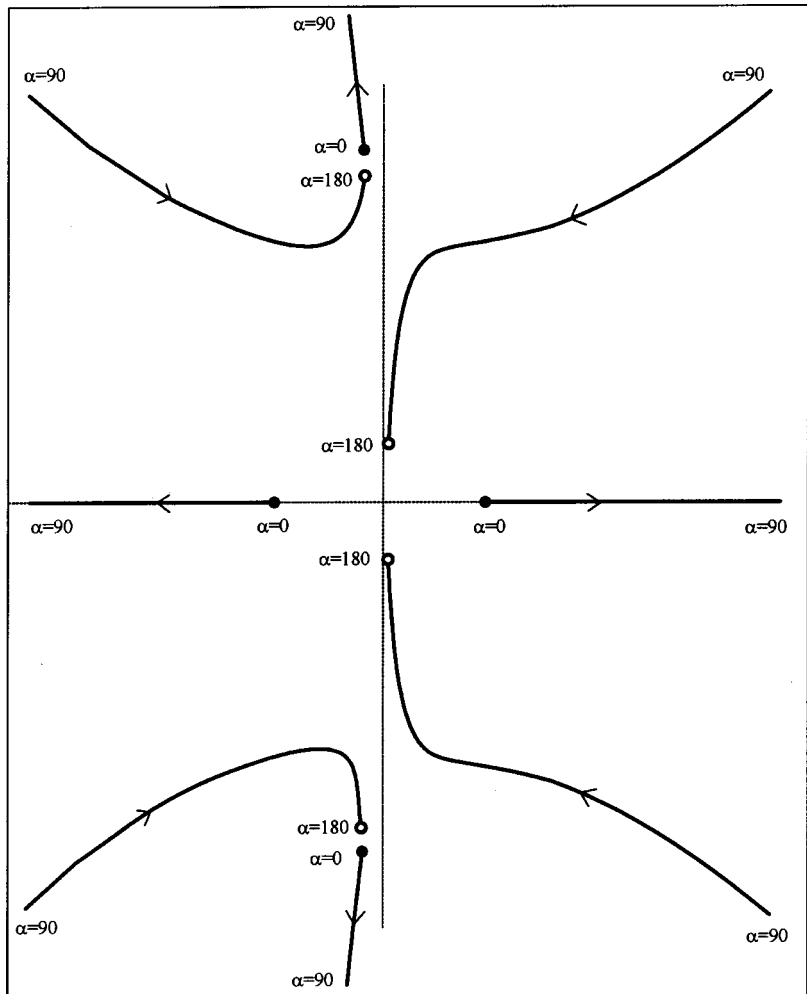
Fig. 4 Locus of motor-tachometer system zeros as angle α varied from 0° to 180°

motor-tachometer-load system are listed in Table 1. These comparisons yet again confirm the validity of the new tachometer model, and justifies its use in system identification and control system design.

We shall now consider the closed-loop system characteristics, first without the tachometer dynamics, and then with the tachometer dynamics present. For the sake of brevity, the terms poles and zeros have been used to denote complex conjugate poles and complex conjugate zeros, respectively.

If the tachometer dynamics did not exist, the open-loop system transfer function for the motor-tachometer-load system under consideration would represent a classic noncolocated mechanical sys-

tem, as is evident in Fig. 5. This is a case where multiple inertia elements are connected by flexible elements, and while the torque is applied to the motor rotor, angular measurement is made at the tachometer rotor. From previous work [4–6], it is known that, unlike colocated systems, achieving robust stability for noncolocated systems is relatively difficult. In a colocated system, that is not attached to the ground, all poles are preceded by zeros, and hence there is no overall phase loss. But the same does not hold for a noncolocated system, and as seen in the present case, the third pole occurs without a preceding zero, resulting in a phase loss of 180° at ~2230 Hz (Fig. 6). Irrespective of whether the tachometer signal is used for velocity control or position control,
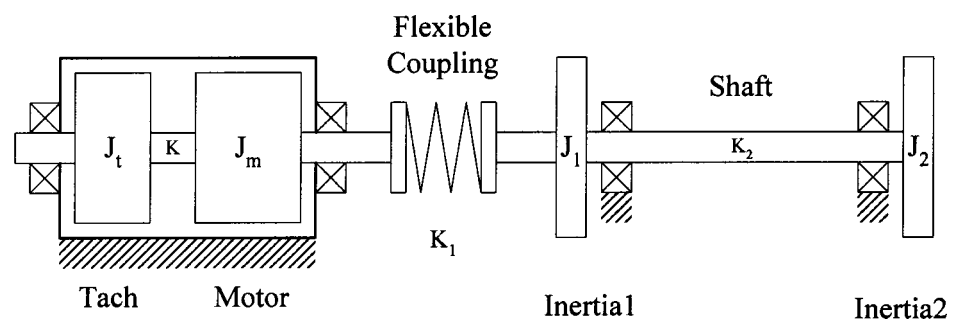
Fig. 5 Motor-tachometer-load system
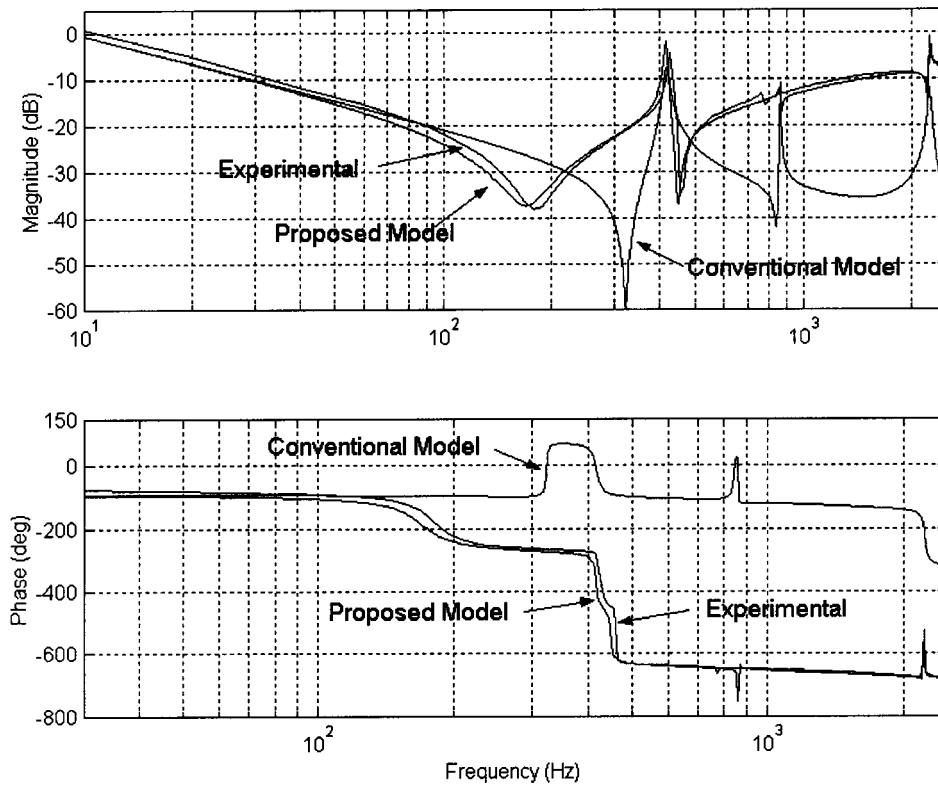
Fig. 6 V_{tach}/V_{in} **Bode plot for the motor-tachometer-load system: Experimental measurement, conventional model, and proposed model**

this last resonance peak determines the stability margins. Higher stability margins, and hence better closed-loop robustness can be achieved if this pole is well damped, a fact that is seen easily from Nyquist plots. In the absence of adequate damping, classical as well as modern control approaches may be used, for example, a low pass filter to attenuate the noncolocated pole, a "notch-filter" compensator [3], a LQG based optimal controller [4], or H-infinity based robust controllers [7,8]. Yet, each scheme has its own disadvantages in terms of control effort, robustness, and sensitivity. Generally speaking, the close-loop performance is limited by the first noncolocated pole frequency, 2230 Hz in this case.

In the case where tachometer dynamics is present, the velocity feedback signal is modified and results in reshuffled open-loop system zeros, some of which are nonminimum phase. This, along with the effects of mechanical compliance in the system, makes the feedback control design for the tachometer-motor-load system yet more challenging. As seen in Fig. 6, apart from losing phase at the pole frequencies, the system also loses phase at the nonminimum phase zero frequencies. It can be deduced from the Nyquist plot of the open-loop system that the cross-over frequency is determined by the location of the first nonminimum phase zero,

which is 178 Hz. In this case, the smaller the damping at zero, the higher is the gain margin. The closed loop bandwidth is now limited by the first nonminimum phase zero frequency. This is due to the fact that the zeros of the open-loop system also appear as the zeros of the closed-loop system, irrespective of the control scheme used. This implies that there will always be a 180° closed-loop phase drop at the nonminimum phase zero frequencies, even if the closed-loop gain stays close to 0 dB until a higher frequency. One may try to compensate for the phase loss at 178 Hz, by adding a minimum phase notch filter controller at a slightly lower frequency. With this strategy, although the closed-loop phase will be restored, the closed-loop gain will drop severely at the zero frequency, once again, limiting the bandwidth. In light of these observations, the zero locus plot presented earlier gains further significance because it is the location of the zeros and not the poles that determines the closed-loop bandwidth of the motor-tachometer-load system.

Apart from bandwidth and stability, other closed-loop performance parameters are also affected in this case. It is well known that a small value for the open-loop sensitivity transfer function is desirable for good disturbance rejection and robustness against

Table 1 Experimentally measured and analytically predicted complex conjugate pole and zero frequencies for the tachometer-motor-load system

Complex conjugate pair	Experimentally measured (Hz)	Analytically predicted using the proposed tachometer model (Hz)	Analytically predicted using the conventional tachometer model (Hz)
Zero	178	170	321
Pole	420	416	416
Zero	455	449	847
Pole	762	860	860
Zero	782	862	
Zero	2200	2217	
Pole	2230	2231	2231

small model parameter variation. Nonminimum phase zeros impose an additional analytic constraint on the sensitivity transfer function—requiring sensitivity to be arbitrarily small over some frequency ranges forces it to be arbitrarily large over other frequency range [13,14]. Furthermore, Fig. 6 also shows that the tachometer dynamics results in large open-loop gains at high frequencies, thus making the system naturally more sensitive to high frequency noise. In summary, the tachometer dynamics not only limits the closed-loop system bandwidth, but also increases the system sensitivity to output disturbances, parameter variations, and high frequency noise.

5 Conclusion

Conventional dc tachometer model is found to be inadequate in predicting the frequency response of an integrated motor-tachometer system. Based on fundamental principles of electromagnetism, an enhanced tachometer model is derived that includes the effects of mutual induction between the motor and tachometer armatures. The tachometer-motor interaction results in complex dynamics that introduces additional nonminimum phase zeros in the loop transfer function. Predictions based on this model are found to agree with the experimental measurements.

The tachometer dynamics identified in this paper is shown to be detrimental to the closed-loop bandwidth and performance. Using conventional control schemes, the system bandwidth is practically limited by the first nonminimum phase zero frequency. Even though well understood, the tachometer dynamics is best avoided due to the complications that it introduces. For two-pole permanent magnet stator dc machines, the derived model provides means for eliminating the tachometer-motor interaction. The two devices can be electromagnetically insulated by means of an appropriate housing design, or the orientation angle α can be set at $\pm 90°$.

Apart from two pole dc machines, various other prevalent electromagnetic actuators and sensors may also be prone to the problems highlighted in this paper. For any of these cases, one would need to conduct a detailed analysis, analogous to the one presented. Such an analysis will depend on the number of stator poles, arrangement of armature windings, and relative placement of the sensor and actuator, among other factors. For example, in a multiple stator pole dc motor, there exists an alternating sequence of radially positive and radially negative armature fields along the periphery of the rotor. Such a distribution may result in a net zero field as seen by a tachometer placed at large distances from the motor, and therefore the coupling effect will be minimal. On the other hand, if the two are placed closely, the possibility of an electromagnetic interaction is high and there will be no orientation α for which the flux linkage between the two coils is zero. Thus, for any given device or system, the sensor-actuator interaction has to be carefully investigated, both analytically as well as experimentally.

Nomenclature

Bold symbols represent vector quantities and corresponding nonbold symbols represent the respective magnitudes of the vector quantities, for example, A_1 is the magnitude of the vector $\boldsymbol{A_1}$.

$\boldsymbol{A_1}$ = area vector of the motor armature
$\boldsymbol{A_2}$ = area vector of the tachometer armature
J_m = motor armature inertia
J_t = tachometer armature inertia
J_i = ith inertia element
K_{amp} = amplifier voltage-to-current gain
K_{b_motor} = motor back emf constant
K_{b_tach} = tachometer back emf constant
K_{t_motor} = motor torque constant
K_{t_tach} = tachometer torque constant
N_1 = number of motor armature coils
N_2 = number of tachometer armature coils
T_{motor} = torque produced by the motor
T_{tach} = torque consumed by the tachometer
K = stiff of the motor-tachometer shaft
K_i = stiffness of ith spring element
V_{in} = voltage input to the amplifier
V_{tach} = tachometer output voltage
θ_i = angle of ith inertia element
θ_m = motor angle
θ_t = tachometer angle
ω_m = motor angular velocity
ω_t = tachometer angular velocity
τ_{amp} = amplifier time constant

References

[1] Awtar S., 2000, "Magnetic Coupling Between DC Motor and Tachometer and Its Effect on Motion Control in the Presence of Shaft Compliance," M.S. thesis, Rensselaer Polytechnic Institute, Troy, NY.

[2] Ogata, K., 1998, *Modern Control Engineering*, Prentice Hall, Upper Saddle River, NJ.

[3] Franklin, G. F., and Powell, J. D., 1994, *Feedback Control of Dynamic Systems*, Addison-Wesley, Reading, MA.

[4] Martin, G. D., 1978, "On the Control of Flexible Mechanical Systems," Ph.D. dissertation, Stanford University, Stanford, CA.

[5] Cannon, R. H., Jr., and Rosenthal, D. E., 1984, "Experiments in Control of Flexible Structures With Noncolocated Sensors and Actuators," J. Guidance, **7**, pp. 546–553.

[6] Spector, V., and Flashner, H., 1990, "Modeling and Design Implications of Noncolocated Control in Flexible Systems," ASME J. Dynamics Syst. Measure. and Contr., **112**, pp. 186–163.

[7] Karkoub, M., Balas, G., Tamma, K., and Donath, M., 2000, "Robust Control of Flexible Manipulators Via μ Synthesis," Control Eng. Pract., **8**, pp. 725–734.

[8] Chiang, R. Y., and Safonov, M. G., 1990, "H-Infinity Robust Controller for an Undamped, Noncolocated, Spring–Mass System," Proceedings of the American Control Conference, pp. 966–967.

[9] McLean, D., 1978, "Mathematical Models of Electrical Machines," Meas. Control, **11**, pp. 231–236.

[10] Fitzgerald, A. E., and Kingsley, C., 1961, *Electric Machinery: The Dynamics and Statics of Electromechanical Energy Conversion*, McGraw-Hill, New York, NY.

[11] Wildi, T., 1997, *Electrical Machines, Drives and Power Systems*, Prentice Hall, Upper Saddle River, NJ.

[12] De France, J. J., 1983, *Electrical Fundamentals*, Prentice-Hall Inc., Eaglewood Cliffs, NJ.

[13] Freudenberg, J. S., and Looze, D. P., 1985, "Right Half Plane Poles and Zeros and Design Tradeoffs in Feedback Systems," IEEE Trans. Autom. Control, **AC-30**, pp. 555–565.

[14] Middleton, R. H., 1991, "Trade-Offs in Linear Control System Design," Automatica, **27**, pp. 281–292.